

Thermodynamic, Dynamic and Structural Anomalies for Shoulder-like potentials

Ney M. Barraz Jr. and Evy Salcedo

*Instituto de Física, Universidade Federal do Rio Grande do Sul,
Caixa Postal 15051, 91501-970, Porto Alegre, RS, Brazil*

Marcia C. Barbosa

*Instituto de Física, Universidade Federal do Rio Grande do Sul
Caixa Postal 15051, 91501-970, Porto Alegre, Rio Grande do Sul*

(Dated: August 5, 2009)

Abstract

Using molecular dynamic simulations we study a family of continuous core-softened potentials consisting of a hard core, a shoulder at closest distances and an attractive well at further distance. The repulsive shoulder and the well distances represent two length scales. We show that if the first scale, the shoulder, is repulsive or has a small well, the potential has a region in the pressure-temperature phase diagram with density, diffusion and structural anomalies. However, if the closest scale becomes a deep well the regions in the pressure-temperature phase diagram where the three anomalies are present shrink and disappear. This result helps in defining two length scales potentials that exhibits anomalies.

PACS numbers: 64.70.Pf, 82.70.Dd, 83.10.Rs, 61.20.Ja

I. INTRODUCTION

Most liquids contract upon cooling. This is not the case of water, a liquid where the specific volume at ambient pressure starts to increase when cooled below $T \approx 4^\circ\text{C}$ ^{1,2}. Besides, in a certain range of pressures, water also exhibits an anomalous increase of compressibility and specific heat upon cooling³⁻⁵. Experiments for Te,⁶ Ga, Bi,⁷ S,^{8,9} and Ge₁₅Te₈₅,¹⁰ and simulations for silica,¹¹⁻¹⁴ silicon¹⁵ and BeF₂,¹¹ show the same density anomaly.

Water also has dynamic anomalies. Experiments show that the diffusion constant, D , increases on compression at low temperature, T , up to a maximum $D_{\text{max}}(T)$ at $p = p_{D_{\text{max}}}(T)$. The behavior of normal liquids, with D decreasing on compression, is restored in water only at high p , e.g. for $p > p_{D_{\text{max}}} \approx 1.1$ kbar at 10°C ^{2,3}. Numerical simulations for SPC/E water¹⁶ recover the experimental results and show that the anomalous behavior of D extends to the metastable liquid phase of water at negative pressure, a region that is difficult to access for experiments¹⁷⁻²⁰. In this region the diffusivity D decreases for decreasing p until it reaches a minimum value $D_{\text{min}}(T)$ at some pressure $p_{D_{\text{min}}}(T)$, and the normal behavior, with D increasing for decreasing p , is reestablished only for $p < p_{D_{\text{min}}}(T)$ ^{17-19,21}. Besides water, silica^{13,22} and silicon²³ also exhibit a diffusion anomalous region.

It was proposed a few years ago that these anomalies are related to a second critical point between two liquid phases, a low density liquid (LDL) and a high density liquid (HDL)²⁴. This critical point was discovered by computer simulations. This work suggests that this critical point is located at the supercooled region beyond the line of homogeneous nucleation and thus cannot be experimentally measured. Even with this limitation, this hypothesis has been supported by indirect experimental results^{25,26}.

In order to describe the anomalies present in water and in other liquids, isotropic models has been used as the simplest framework to understand the physics of the liquid-liquid phase transition and liquid state anomalies. From the desire of constructing a simple two-body isotropic potential capable of describing the complicated behavior present in water-like molecules, a number of models in which single component systems of particles interact via core-softened potentials²⁷ have been proposed. They possess a repulsive core that exhibits a region of softening where the slope changes dramatically. This region can be a shoulder or a ramp²⁸⁻⁴⁹. These models exhibit density, diffusion and structural anomalies, but depending on the specific shape of the potential, the anomalies might be hidden in the metastable and

unstable phases⁴⁹. The relation between the specific shape of the core-softened potential and the presence or not of the anomalies is still missing.

How the specific shape of a core-softened potential affects the location of the anomalies and the critical points? In order to answer to this question in this paper we analyze a family of continuous core-softened potentials that exhibit two length scales, a shoulder followed by an attractive well. When the shoulder is purely repulsive, this core-softened potential represents the effective pair interaction between two neighbors tetramers^{44,50} and the density, the diffusion and the structural anomalies are present^{44,45}. If the shoulder has a deep well with attractive forces, this potential it is related to the effective interaction potential between two water molecules obtained from the ST4⁵¹ or TIP5P⁵² models for water. In this case the effective potential is derived from the oxygen-oxygen radial distributions function, solving the Ornstein-Zernike equation by using an integral equation method^{51,52}. The resulting potential has a shoulder with a deep well at closest distance and a second well with lower energy at furthest distance. The detailed depth of the softening region depends on the approximations employed. This potential leads, as we are going see in this paper, to systems in which the anomalies are in the unstable region of the phase diagram while in the full ST4 and TIP5P systems the anomalies can be observed. It is important, therefore, to understand what is lost when one goes from the specific anisotropic ST4 and TIP5P potentials to the isotropic spherical symmetric case.

So, in this paper we study what happens with the region in the pressure-temperature phase diagram where the anomalies are located as the potential changes from a repulsive shoulder to a very deep well. Our results will shade some light not only in the use of spherical symmetric approximations of asymmetric potentials but also will help to design potentials for new systems with anomalies.

The paper is organized as follows. In sec. II the family of potentials is introduced and its link with the derivation the framework of the integral equations is presented. In sec. III these potentials are tested for presence density, diffusion and structural anomalies, and for the the existence of two liquid phases and a critical points by molecular dynamic simulations. Conclusions are presented in sec. IV.

II. THE MODEL

We study a system of N particles, with diameter σ , where the pair interaction is described by a family of continuous potentials given by

$$U(r) = \epsilon \left[\left(\frac{\sigma}{r} \right)^a - \left(\frac{\sigma}{r} \right)^b \right] + \sum_{j=1}^4 h_j \exp \left[- \left(\frac{r - c_j}{w_j} \right)^2 \right] . \quad (1)$$

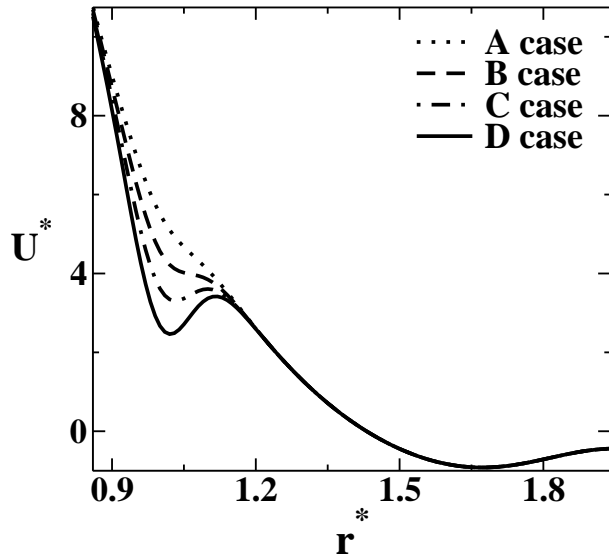


FIG. 1: Interaction potential obtained by changing parameters h_1 in Eq. (1). The potential and the distances are in dimensionless units $U^* = U/\gamma$ and $r^* = r/r_0$.

The first term is a Lennard-Jones potential-like and the second one is composed by four Gaussians, each one centered in c_j . This potential can represent a whole family of intermolecular interactions, depending of the choice of the parameters $a, b, \sigma, \{h_j, c_j, w_j\}$, with $j = 1, \dots, 4$. The parameters are chosen in order to obtain a two length scale potential⁵¹.

In order to make the simulations in dimensionless units, the potential and the distances are given in dimensionless units, $U^* = U/\gamma$ and $r^* = r/r_0$ where γ is the energy scale and r_0 is the length scale chosen so the closest approach between particles is about $r^* = 1$. All the parameters of the model are used in the simulations in units of γ and r_0 . In this work $\epsilon/\gamma = 0.02$ and $\sigma/r_0 = 1.47$. Modifying h_1 in the Eq. 1 allow us to change the depth of the hard-core well, as illustrated in Fig. 1. Here we use four different values for h_1 and they are expressed as a multiple of a reference value h_1^{ref} as shown in the Table I. For all the four cases the values of $a, b, \{c_j, w_j\}$ with $j = 1, \dots, 4$ and h^{ref} . Table II gives the parameter

values in \AA and $kcal/mol$ consistent with modeling ST4 water⁵¹. The depth of the region of softening of the potentials illustrated in the Fig. 1 where chosen so that the potential B is the shallow shoulder-like potential similar to the one studied by de Oliveira et al.⁴⁴ that exhibits the anomalies, while for the potential D the region of softening has the same depth as the potential obtained by using the oxygen-oxygen radial distribution function for the ST4 model⁵¹. In this case, the shoulder region has attractive forces. For comparison we also analyzed two other cases: potential A with a ramp-like shoulder and potential C , with a very shallow shoulder.

The properties of the system were obtained by NVT molecular dynamics using Nose-Hoover heat-bath with coupling parameter $Q = 2$. The system is characterized by 500 particles in a cubic box with periodic boundary conditions, interacting with the intermolecular potential described above. All physical quantities are expressed in reduced units and defined as

$$\begin{aligned} t^* &= \frac{t(m/\gamma)^{1/2}}{r_0} \\ T^* &= \frac{k_B T}{\gamma} \\ p^* &= \frac{pr_0}{\gamma} \\ \rho^* &= \rho r_0^3 \\ D^* &= \frac{Dm}{\gamma r_0^2} . \end{aligned}$$

Standard periodic boundary conditions together with predictor-corrector algorithm were used to integrate the equations of motion with a time step $\Delta t^* = 0.002$ and potential cut off radius $r_c^* = 3.5$. The initial configuration is set on solid or liquid state and, in both cases, the equilibrium state was reached after $t_{eq}^* = 1000$ (what is in fact 500000 steps since $\Delta t^* = 0.002$) . From this time on the physical quantities were stored in intervals of $\Delta t_R^* = 1$ during $t_R^* = 1000$. The system is uncorrelated after $t_d^* = 10$, from the velocity auto-correlation function. 50 decorrelated samples were used to get the average of the physical quantities. The thermodynamic stability of the system was checked analyzing the dependence of pressure on density, by the behavior of the energy and also by visual analysis of the final structure, searching for cavitation.

TABLE I: Parameters h_1 for potentials A, B, C and D.

Potential	Value of h_1
<i>A</i>	$0.25 h_1^{ref}$
<i>B</i>	$0.50 h_1^{ref}$
<i>C</i>	$0.75 h_1^{ref}$
<i>D</i>	$1.00 h_1^{ref}$

TABLE II: Parameters for potentials A, B, C and D in units of \AA and of $kcal/mol$.

Parameter	Value	Parameter	Value
<i>a</i>	9.056	w_1	0.253
<i>b</i>	4.044	w_2	1.767
ϵ	0.006	w_3	2.363
σ	4.218	w_4	0.614
c_1	2.849	h_1^{ref}	-1.137
c_2	1.514	h_2	3.626
c_3	4.569	h_3	-0.451
c_4	5.518	h_4	0.230

III. RESULTS

Pressure-Temperature Phase Diagram

First, we are going to show the effects of the shoulder depth in the presence or not of the thermodynamic anomalies and the location in the pressure-temperature phase diagram of the different phases. Fig. 2 illustrates the pressure-temperature phase diagram of the four cases. The system at high temperatures has a fluid phase and a gas phase (not shown). These two phases coexist at a first order line that ends at a critical point (see Table III for the pressure and the temperature values). At low temperatures and high pressures there are two liquid phases coexisting at a first order line (not shown) ending at a second critical point (see Table IV for the pressure and the temperature values) that is identified in the graph by the region where isochores cross.

TABLE III: Critical point location for potentials A, B, C and D.

Potential	T_{c1}^*	p_{c1}^*
<i>A</i>	1.93	0.072
<i>B</i>	1.98	0.078
<i>C</i>	2.02	0.080
<i>D</i>	2.15	0.094

TABLE IV: Second critical point location for potentials A, B, C and D.

Potential	T_{c2}^*	p_{c2}^*
<i>A</i>	0.35	3.44
<i>B</i>	0.48	1.86
<i>C</i>	0.57	0.49
<i>D</i>	0.81	-0.33

In the Fig. 2 at low temperatures and low pressures the dotted line separates the fluid phase from the amorphous region. The amorphous region is identified by the diffusion coefficient that becomes zero. For the potential *A*, the amorphous region is located in a pressure range $-0.91 \lesssim p^* \lesssim 3.40$, for *B* case this region is located in the range $-0.89 \lesssim p^* \lesssim 1.80$ and for *C* case it is located in the range $-1.00 \lesssim p^* \lesssim 0.48$. The potential *D* does not have a stable amorphous phase. Hence, as the shoulder becomes deeper the amorphous phase shrinks and moves to a lower pressure range.

At low temperatures and high pressures two liquid phases are present. As the shoulder becomes deeper the liquid-liquid coexistence line slides down to lower pressures and it goes to higher temperatures. This indicates that the deeper the shoulder the liquid-liquid phase transition stays stable for higher temperatures. Therefore, even though this transition only exists if the attractive part of the potential is present (the second length scale), the stability of the liquid phases is determined by the depth of the shoulder (the first length scale).

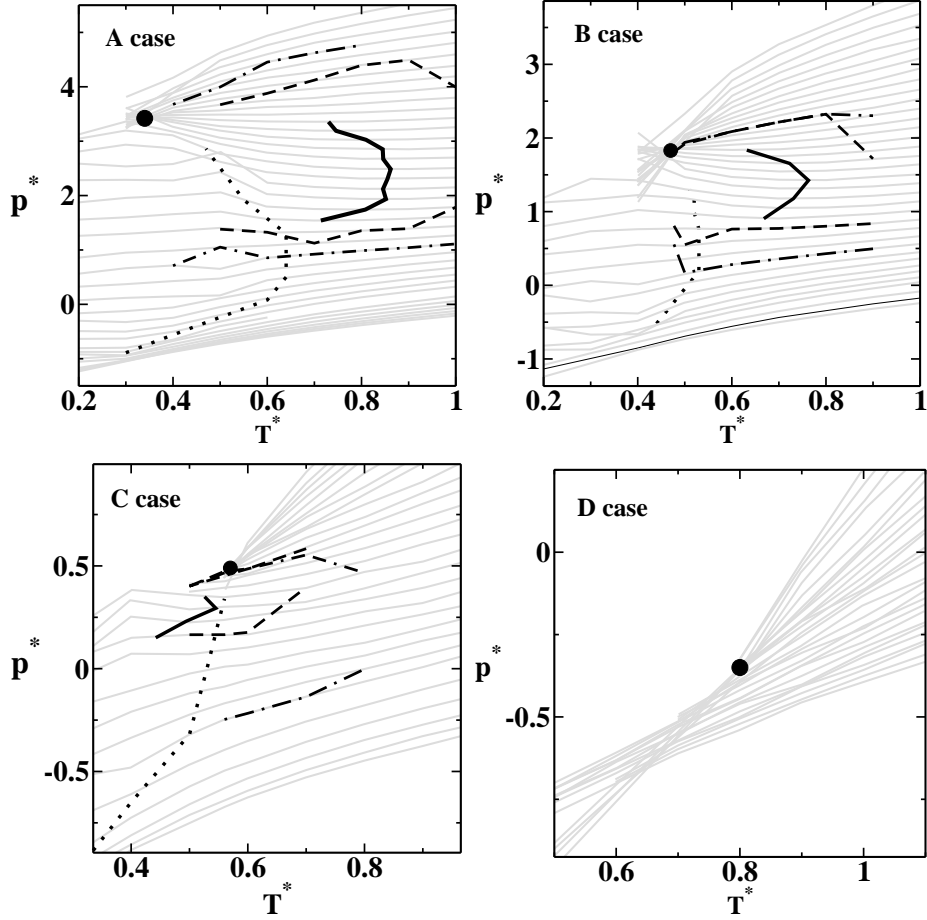


FIG. 2: Pressure-temperature phase diagram for cases *A*, *B*, *C* and *D*. The thin solid lines are the isochores $0.30 < \rho^* < 0.65$. The liquid-liquid critical point is the dot, the temperature of maximum density is the solid thick line, the diffusion extrema is the dashed line and the structural extrema is the dashed-dotted line. The dotted line indicates the limit between the fluid and the amorphous regions.

Thermodynamics anomaly

The Fig. 2 also shows the isochores $0.30 \leq \rho^* \leq 0.65$ represented by thin solid lines. The temperature of maximum density at constant pressure coincides with the minimum pressure on isochores, $\left(\frac{\partial p}{\partial T}\right)_\rho = 0$. From the equation

$$\left(\frac{\partial V}{\partial T}\right)_p = -\left(\frac{\partial p}{\partial T}\right)_V \left(\frac{\partial V}{\partial p}\right)_T \quad (2)$$

is possible to see that, for a fixed density, a minimum in the pressure as a function of temperature represents a maximum in the density as a function of temperature, named

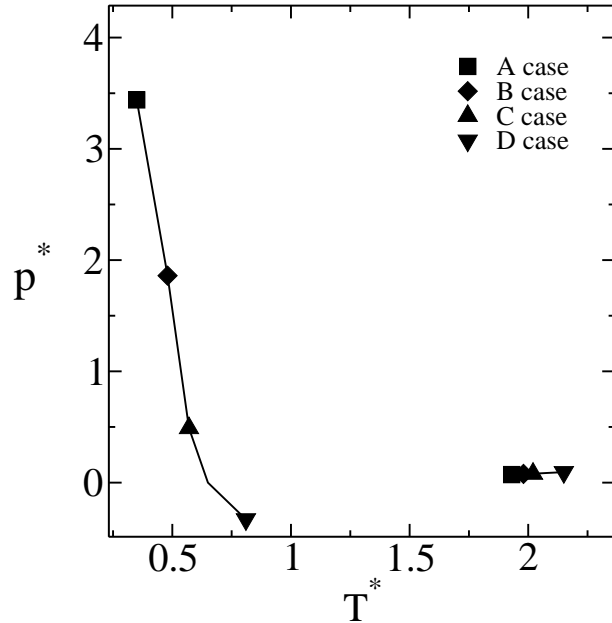


FIG. 3: Location of the critical points on pressure-temperature phase diagram for cases *A*, *B*, *C* and *D*.

temperature of maximum density (TMD) given by $(\frac{\partial V}{\partial T})_p = 0$. The TMD is the boundary of the region of thermodynamic anomaly, where a decrease in the temperature at constant pressure implies an anomalous increase in the density and therefore an anomalous behavior of density (similar to what happens in water). Fig. 2 shows the TMD as a solid thick line. For the potentials *A*, *B* and *C* the TMD is present but for potential *D* no TMD is observed.

Similarly to what happens with the location of amorphous region and of the second critical, as the shoulder becomes deeper, the region in the pressure-temperature phase diagram delimited by the TMD goes to lower pressures, shrinks and disappears for the case *D*, the potential with the deepest shoulder. As the region delimited by the TMD shrinks, it also goes to lower temperatures. For the potential *C* the TMD line is located at temperatures below the the temperature of the liquid-liquid critical point. The thermodynamic parameters that limits the TMD in phase diagram are shown in the Table V, where p_l represents the values of (ρ^*, T^*, p^*) for the point of the lowest pressure in the TMD line, p_m is the point with the highest temperature and p_h is the point with the highest pressure.

The link between the depth of the shoulder and the presence or not of the TMD goes as follows. The TMD is related to the presence of large regions in the system in which particles are in two preferential distances represented by the first scale and the second scale in our

cases	p_l	p_m	p_h	
<i>A</i>	ρ^*	0.47	0.52	0.57
	T^*	0.71	0.85	0.73
	p^*	1.50	2.50	3.30
<i>B</i>	ρ^*	0.46	0.50	0.54
	T^*	0.67	0.76	0.63
	p^*	0.90	1.40	1.80
<i>C</i>	ρ^*	0.40	0.42	0.43
	T^*	0.44	0.54	0.52
	p^*	0.15	0.29	0.36

TABLE V: Limiting values for density (ρ^*), temperature (T^*) and pressure (p^*) of the thermodynamics anomalies on pressure-temperature diagram. Here the point p_l represents the density, temperature and pressure of the point of the lowest pressure in the TMD line, p_m represents the point of the highest temperature and p_h represents the point of the highest pressure of the TMD line.

potential^{49,53-55}. While for normal liquids as the temperature is increased the percentage of particles at closest scales decreases (see case *D* in the Fig. 4), for the anomalous liquid (see cases *A*, *B* and *C* in the Fig. 4) there are a region in the pressure-temperature phase diagram where as the temperature is increased the percentage of particles at the closest distance increases. This increase in the percentage is only possible if particles move from the second to the first scale. In the first case, the decrease of particles in the first scale leads to a decrease of density with increase of temperature, behavior expected for normal liquids. In the second case, the increase of particles in the first scale leads to an increase of density with temperature what characterizes the anomalous region. The anomaly is, therefore, related with the increase of the probability of particles to be in the first scale when the temperature is increased while the percentage of particles in the second scale decreases.

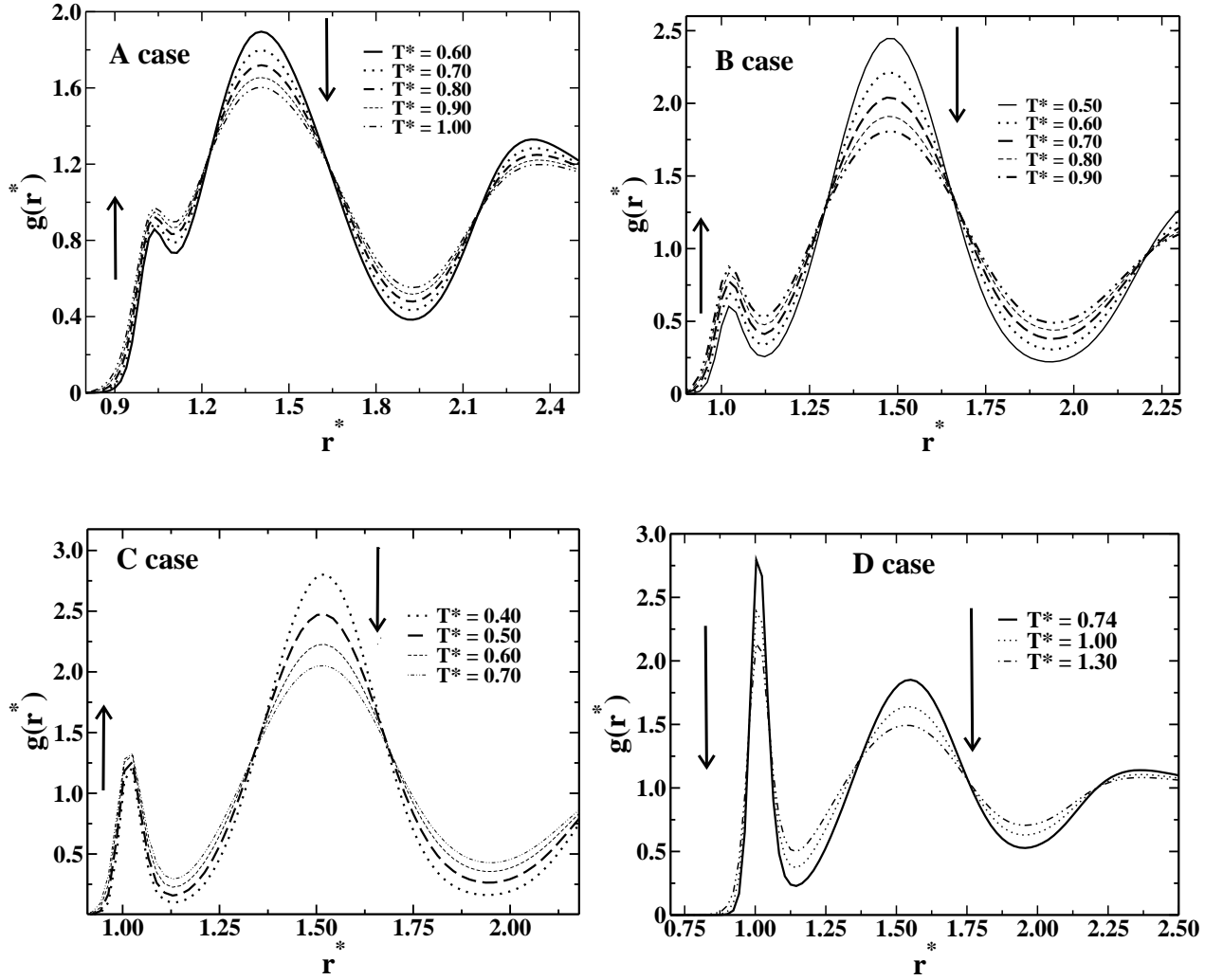


FIG. 4: Radial distribution as a function of the distance for the four potentials. In the cases *A*, *B* and *C* the first peak of $g(r^*)$ increases with the increase of the temperature, while the second peak decreases. For the potential *D* all the peaks decrease with the increase of the temperature.

Diffusion anomaly

Now we are going to test the effect the shoulder depth has in the location of the diffusion anomaly in the pressure temperature phase diagram. The diffusion coefficient is obtained from the expression:

$$D = \lim_{t \rightarrow \infty} \frac{\langle [\vec{r}_j(t_0 + t) - \vec{r}_j(t_0)]^2 \rangle_{t_0}}{6t} \quad (3)$$

where $\vec{r}_j(t)$ are the coordinates of particle j at time t , and $\langle \dots \rangle_{t_0}$ denotes an average over all particles and over all t_0 .

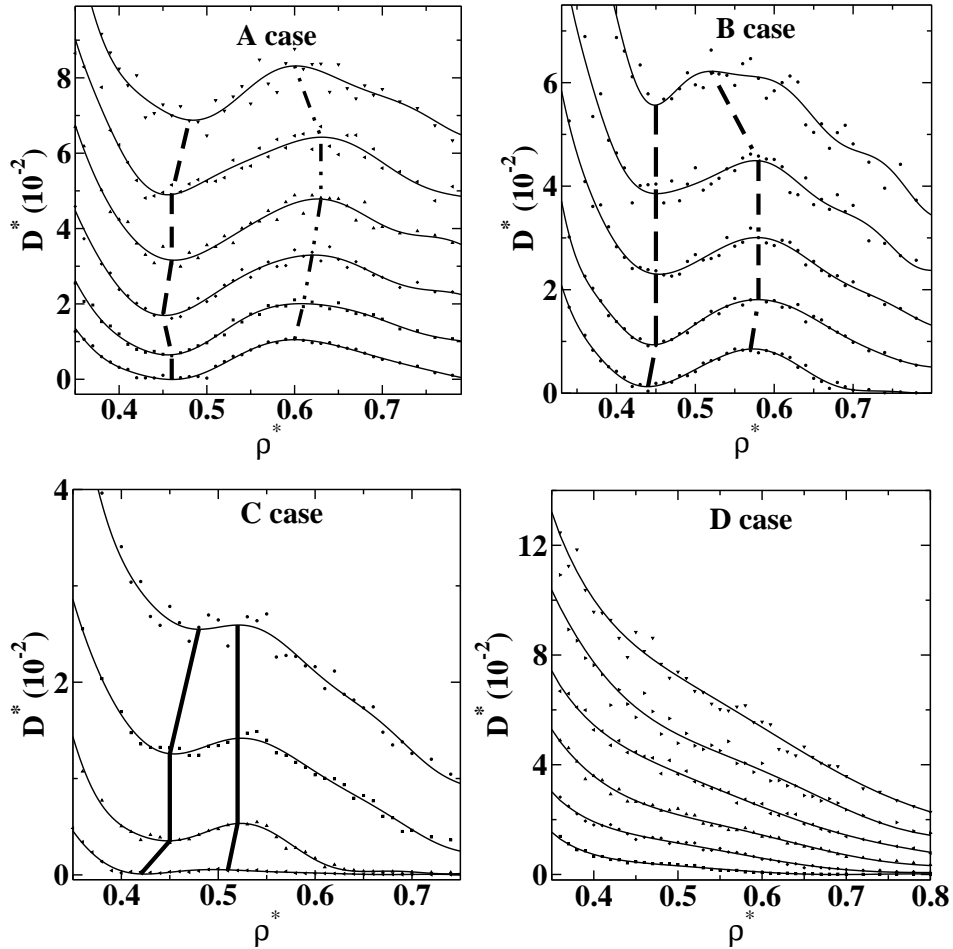


FIG. 5: Diffusion coefficient as a function of density. The dots are the simulational data and the solid lines are polynomial fits. The dashed lines connect the densities of minima and maxima diffusivity that limit the diffusion anomalous region.

Fig. 5 shows the behavior of the dimensionless translational diffusion coefficient, D^* , as function of the dimensionless density, ρ^* , at constant temperature for the four cases. The solid lines are a polynomial fits to the data obtained by simulation (the dots in the Fig. 5). For normal liquids, the diffusion at constant temperature increases with the decrease of the density. For the potentials A , B and C the diffusion has a region in the pressure-temperature phase diagram in which the diffusion increases with density. This is the diffusion anomalous region. In the Fig. 5 one dashed line joints the points of the density (or pressure) of minimum diffusion for different temperatures and another dashed line links the points of density (or pressure) of maximum diffusion for different temperatures.

Similarly to what happens with the location of the TMD, as the shoulder becomes deeper,

the region in the pressure-temperature phase diagram delimited by the extrema of the diffusion goes to lower pressures, shrinks and disappears for the case D , the potential with the deepest shoulder.

Fig. 2 shows the location at the pressure-temperature phase diagram of the pressure of maximum and minimum diffusion as dashed lines (the dashed lines in the Fig. 5). In the Fig. 2 we show that in the pressure-temperature phase diagram the region where the dynamic anomaly occurs englobes the region where the thermodynamic anomaly is present. This hierarchy between the anomalies is observed in a number of models^{17,18,47} and in the water.²

The link between the depth of the shoulder and the presence or not of the region of diffusion extrema goes as follows. The presence of the diffusion anomaly is related to having the quantity $\Sigma_2 > 0.42$ ^{47,56} where

$$\begin{aligned}\Sigma_2 &= \left(\frac{\partial s_2}{\partial \ln \rho} \right)_T \\ &= s_2 - 2\pi\rho^2 \int \ln g(r) \frac{\partial g(r)}{\partial \rho} r^2 dr\end{aligned}\quad (4)$$

where

$$s_2 = -2\pi\rho \int [g(r) \ln g(r) - g(r) + 1] r^2 dr , \quad (5)$$

is the excess entropy. Fig. 6 illustrates the behavior of the radial distribution function for fixed temperature as the density varies. For the case A the $\ln g(r)$ is negative and $dg(r)/d\rho$ is positive for the first scale, while for the second scale the $\ln g(r)$ is positive and the $dg(r)/d\rho$ is negative. As a result the second parcel in Eq. (5) is positive a requirement for having $\Sigma_2 > 0.42$ since s_2 is negative⁴⁷. For case D, also shown in Fig. 6, the $\ln g(r)$ is positive and huge and $dg(r)/d\rho$ is positive what leads to a second parcel in Eq. (5) that is negative what do not fulfill the requirement $\Sigma_2 > 0.42$.

Structural anomaly

Finally we are going to test the effect the shoulder depth has in the location in the pressure-temperature phase diagram of the structural anomalous region.

The translational order parameter is defined as^{13,18,57}

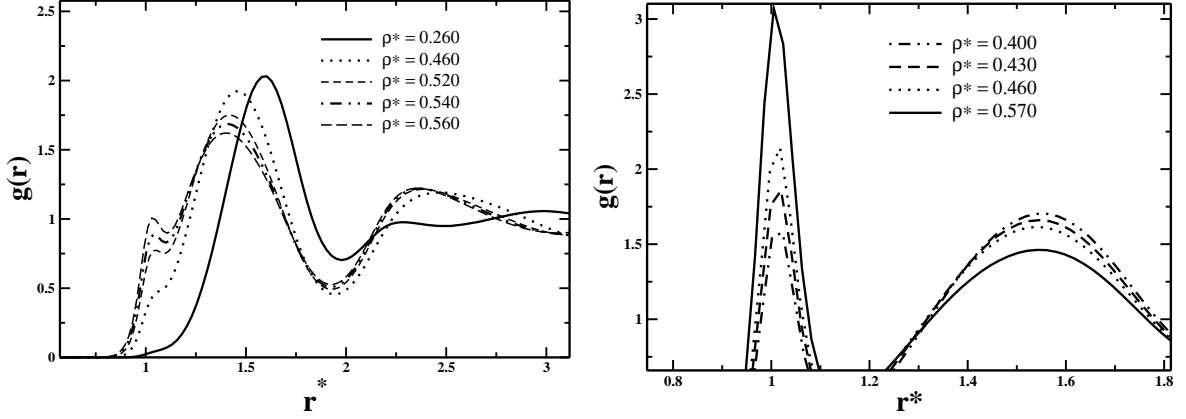


FIG. 6: Radial distribution for cases A and D as a function of r^* for various densities. In the case A the temperature is fixed $T^* = 0.90$ while in the case D the temperature is $T^* = 1.10$.

$$t = \int_0^{\xi_c} |g(\xi) - 1| d\xi \quad (6)$$

where $\xi = r\rho^{\frac{1}{3}}$ is the distance r in units of the mean interparticle separation $\rho^{-\frac{1}{3}}$, ξ_c is the cutoff distance set to half of the simulation box times⁴⁵ $\rho^{-\frac{1}{3}}$, $g(\xi)$ is the radial distribution function proportional to the probability of finding a particle at a distance ξ from a referent particle. The translational order parameter measure how structured is the system. For an ideal gas $g = 1$ and $t = 0$, and the case of crystal phase $g \neq 1$ over long distances and t is large. Therefore for normal fluids t increases with the increase of the density.

Fig. 7 shows the translational order parameter as a function of the density for fixed temperatures. The dots represent the simulation data and the solid line the polynomial fit to the data. For the potentials A , B and C there are a region of densities in which the translational parameter decreases as the density increases. A dotted-dashed line illustrates the region of local maximum of t^* and minimum of t^* limiting the anomalous region. For the potential D , t^* increases with the density. No anomalous behavior is observed.

Fig. 2 shows the structural anomaly for cases A , B and C , as dotted-dashed lines. It is observed that the region of structural anomaly embraces both dynamic and thermodynamic anomalies. Similarly to other anomalies the effect of increase the depth of the repulsive shoulder is to narrow the anomalies asymmetrical. The branch of anomaly in pressures near to liquid-liquid critical point is most feeling to the effect of the shoulder compared with the branch obtained in low pressures. However, the hierarchy of the anomalies is maintained,

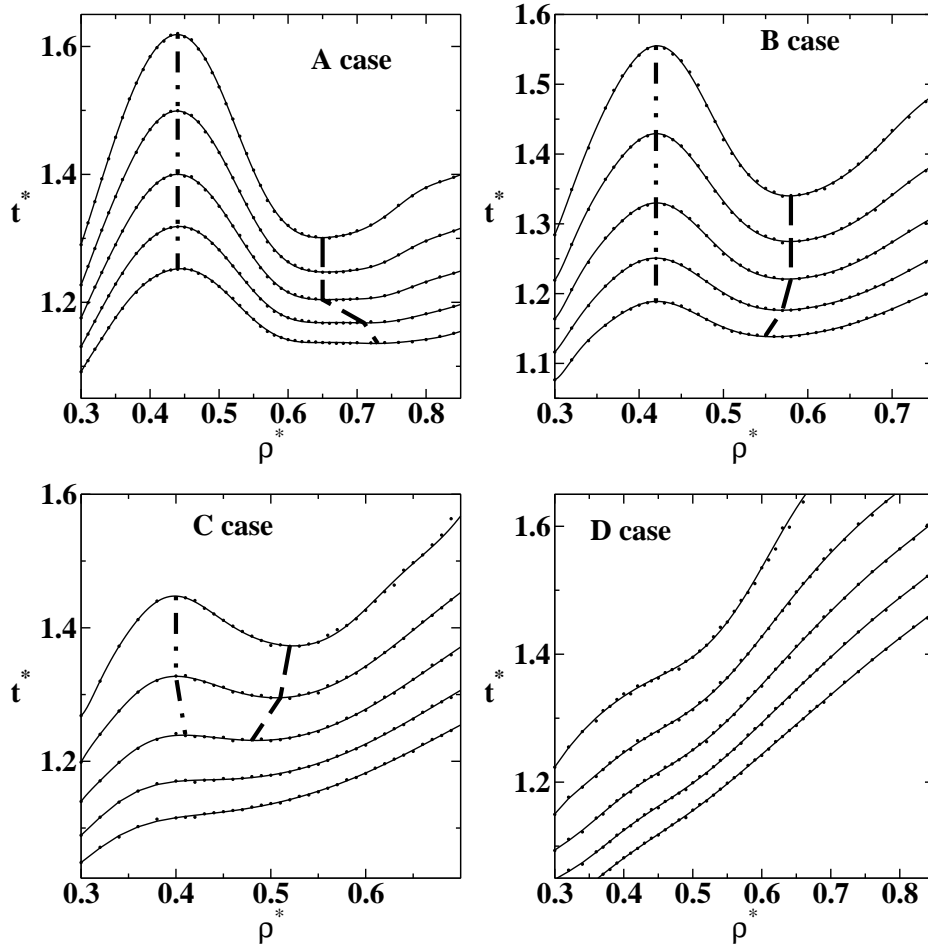


FIG. 7: The translational order parameter as a function of density for fixed temperatures: $T^* = 1.10, 1.00, 0.90, 0.80, 0.70$ and 0.60 (from top to bottom). The dot-dashed lines locate the density of maxima e minima t^* .

the change in the repulsive shoulder does not affect it.

IV. CONCLUSIONS

In this paper we studied a family of potentials characterized by two length scales: a shoulder and an attractive well. We analyzed the effect in the location in the pressure-temperature phase diagram of the density, diffusion and structural anomalies of making this repulsive shoulder a deep well. We found that the anomalies shrink and disappear as the well becomes deeper. This indicates that an important mechanism for the anomalies is the possibility of particles in the furthest length scale to move to the closest length scale. As the shoulder well becomes deeper particles becomes localized in the closest scale and the

mobility between the two scales decreases.

We find that in the cases of potentials A , B and C the thermodynamic, dynamic and structural anomalies are present and that the region of structural anomaly embraces the dynamic and thermodynamic anomaly in pressure-temperature phase diagram. This implies that the hierarchy of the anomalies is preserved independent of the depth of the repulsive shoulder, however when the shoulder becomes deeper, the upper pressure lines of anomaly converge to a similar value in the pressure-temperature phase diagram.

What is the connection between the studies potentials and the real system? Effective potentials for water has been derived based in the oxygen-oxygen radial distribution function for the ST4⁵¹ and TIP5P⁵² models for water. In both cases the effective potential was obtained from the $g(r^*)$ using the Ornstein-Zernike equation and integral equation approximations. The potential resulting are the case D in the Fig. 1 in the case of ST4 and for the TIP5P model a potential that exhibits a deep shoulder similar to the case D . Consequently the approximation washes out the anomalies present in both ST4 and TIP5P. In the case of the TIP5P it was shown that if instead of deep shoulder a smooth shoulder like the one present in the ramp potential would be used, the anomalies not only would be present but would be located in the same region of pressure and temperature of the TIP5P potential.

In resume, similarly to other previous studies^{40,44,58,59}, a directional interaction potential is not a fundamental ingredient to have a water-like anomalies. Two scales isotropic potential also reproduce this anomalies if the shoulder closest scale would not be too deep.

ACKNOWLEDGMENTS

We thank for financial support the Brazilian science agencies CNPq and Capes. This work is partially supported by CNPq, INCT-FCx.

¹ R. Waler, *Essays of natural experiments* (Johnson Reprint, New York, 1964).

² C. A. Angell, E. D. Finch, and P. Bach, *J. Chem. Phys.* **65**, 3063 (1976).

- ³ F. X. Prielmeier, E. W. Lang, R. J. Speedy, and H.-D. Lüdemann, *Phys. Rev. Lett.* **59**, 1128 (1987).
- ⁴ F. X. Prielmeier, E. W. Lang, R. J. Speedy, and H.-D. Lüdemann, *Ber. Bunsenges. Phys. Chem.* **92**, 1111 (1998).
- ⁵ L. Haar, J. S. Gallagher, and G. Kell, *NBS/NRC Steam Tables. Thermodynamic and Transport Properties and Computer Programs for Vapor and Liquid States of Water in SI Units.* (Hemisphere Publishing Co., Washington D. C., 1984), 1st ed.
- ⁶ H. Thurn and J. Ruska, *J. Non-Cryst. Solids* **22**, 331 (1976).
- ⁷ *Periodic table of the elements*, <http://periodic.lanl.gov/default.htm> (2007).
- ⁸ G. E. Sauer and L. B. Borst, *Science* **158**, 1567 (1967).
- ⁹ S. J. Kennedy and J. C. Wheeler, *J. Chem. Phys.* **78**, 1523 (1983).
- ¹⁰ T. Tsuchiya, *J. Phys. Soc. Jpn.* **60**, 227 (1991).
- ¹¹ C. A. Angell, R. D. Bressel, M. Hemmatti, E. J. Sare, and J. C. Tucker, *Phys. Chem. Chem. Phys.* **2**, 1559 (2000).
- ¹² R. Sharma, S. N. Chakraborty, and C. Chakravarty, *J. Chem. Phys.* **125**, 204501 (2006).
- ¹³ M. S. Shell, P. G. Debenedetti, and A. Z. Panagiotopoulos, *Phys. Rev. E* **66**, 011202 (2002).
- ¹⁴ P. H. Poole, M. Hemmati, and C. A. Angell, *Phys. Rev. Lett.* **79**, 2281 (1997).
- ¹⁵ S. Sastry and C. A. Angell, *Nature Mater.* **2**, 739 (2003).
- ¹⁶ H. J. C. Berendsen, J. R. Grigera, and T. P. Straatsma, *J. Phys. Chem.* **91**, 6269 (1987).
- ¹⁷ P. A. Netz, F. W. Starr, H. E. Stanley, and M. C. Barbosa, *J. Chem. Phys.* **115**, 344 (2001).
- ¹⁸ J. R. Errington and P. G. Debenedetti, *Nature (London)* **409**, 318 (2001).
- ¹⁹ J. Mittal, J. R. Errington, and T. M. Truskett, *J. Phys. Chem. B* **110**, 18147 (2006).
- ²⁰ P. Kumar, G. Franzese, and H. E. Stanley, *Phys. Rev. E* **73**, 041505 (2006).
- ²¹ A. Mudi, C. Chakravarty, and R. Ramaswamy, *J. Chem. Phys.* **122**, 104507 (2005).
- ²² S. H. Chen, F. Mallamace, C. Y. Mou, M. Broccio, C. Corsaro, A. Faraone, and L. Liu, *Proceedings of the National Academy of Science of United States of America* **103**, 12974 (2006).
- ²³ T. Morishita, *Phys. Rev. E* **72**, 021201 (2005).
- ²⁴ P. H. Poole, F. Sciortino, U. Essmann, and H. E. Stanley, *Nature (London)* **360**, 324 (1992).
- ²⁵ O. Mishima and H. E. Stanley, *Nature (London)* **396**, 329 (1998).
- ²⁶ R. J. Speedy and C. A. Angell, *Journal of Chem. Phys.* **65**, 851 (1976).
- ²⁷ P. G. Debenedetti, *J. Phys.: Cond. Matter* **15**, R1669 (2003).

- ²⁸ A. Scala, M. R. Sadr-Lahijany, N. Giovambattista, S. V. Buldyrev, and H. E. Stanley, *J. Stat. Phys.* **100**, 97 (2000).
- ²⁹ G. Franzese, G. Malescio, A. Skibinsky, S. V. Buldyrev, and H. E. Stanley, *Nature (London)* **409**, 692 (2001).
- ³⁰ S. V. Buldyrev, G. Franzese, N. Giovambattista, G. Malescio, M. R. Sadr-Lahijany, A. Scala, A. Skibinsky, and H. E. Stanley, *Physica A* **304**, 23 (2002).
- ³¹ S. V. Buldyrev and H. E. Stanley, *Physica A* **330**, 124 (2003).
- ³² A. Skibinsky, S. V. Buldyrev, G. Franzese, G. Malescio, and H. E. Stanley, *Phys. Rev. E* **69**, 061206 (2005).
- ³³ G. Franzese, G. Malescio, A. Skibinsky, S. V. Buldyrev, and H. E. Stanley, *Phys. Rev. E* **66**, 051206 (2002).
- ³⁴ A. Balladares and M. C. Barbosa, *J. Phys.: Cond. Matter* **16**, 8811 (2004).
- ³⁵ A. B. de Oliveira and M. C. Barbosa, *J. Phys.: Cond. Matter* **17**, 399 (2005).
- ³⁶ V. B. Henriques and M. C. Barbosa, *Phys. Rev. E* **71**, 031504 (2005).
- ³⁷ V. B. Henriques, N. Guissoni, M. A. Barbosa, M. Thielo, and M. C. Barbosa, *Mol. Phys.* **103**, 3001 (2005).
- ³⁸ P. C. Hemmer and G. Stell, *Phys. Rev. Lett.* **24**, 1284 (1970).
- ³⁹ E. A. Jagla, *Phys. Rev. E* **58**, 1478 (1998).
- ⁴⁰ N. B. Wilding and J. E. Magee, *Phys. Rev. E* **66**, 031509 (2002).
- ⁴¹ S. Maruyama, K. Wakabayashi, and M. Oguni, *Aip Conf. Proceedings* **708**, 675 (2004).
- ⁴² R. Kurita and H. Tanaka, *Science* **206**, 845 (2004).
- ⁴³ L. Xu, P. Kumar, S. V. Buldyrev, S.-H. Chen, P. Poole, F. Sciortino, and H. E. Stanley, *Proc. Natl. Acad. Sci. U.S.A.* **102**, 16558 (2005).
- ⁴⁴ A. B. de Oliveira, P. A. Netz, T. Colla, and M. C. Barbosa, *J. Chem. Phys.* **124**, 084505 (2006).
- ⁴⁵ A. B. de Oliveira, P. A. Netz, T. Colla, and M. C. Barbosa, *J. Chem. Phys.* **125**, 124503 (2006).
- ⁴⁶ A. B. de Oliveira, M. C. Barbosa, and P. A. Netz, *Physica A* **386**, 744 (2007).
- ⁴⁷ A. B. de Oliveira, P. A. Netz, and M. C. Barbosa, *Euro. Phys. J. B* **64**, 48 (2008).
- ⁴⁸ A. B. de Oliveira, G. Franzese, P. A. Netz, and M. C. Barbosa, *J. Chem. Phys.* **128**, 064901 (2008).
- ⁴⁹ A. B. de Oliveira, P. E. Netz, and M. C. Barbosa, *Europhys. Lett.* **85**, 36001 (2009).
- ⁵⁰ W. P. Krekelberg, J. Mittal, V. Ganesan, and T. M. Truskett, *Phys. Rev. E* **77**, 041201 (2008).

- ⁵¹ T. Head-Gordon and F. H. Stillinger, *J. Chem. Phys.* **98**, 3313 (1993).
- ⁵² Z. Y. Yan, S. V. Buldyrev, P. Kumar, N. Giovambattista, and H. E. Stanley, *Phys. Rev. E* **77**, 042201 (2008).
- ⁵³ H. E. Stanley, S. V. Buldyrev, M. Canpolat, M. Meyer, O. Mishima, M. R. Sadr-Lahijany, A. Scala, and F. W. Starr, *Physica A* **257**, 213 (1998).
- ⁵⁴ H. E. Stanley, [Proceedings of the 1998 International Conference on Complex Fluids], *Pramana* [A Journal of the Indian Academy of Sciences, founded by C. V. Raman] **53**, 53 (1999).
- ⁵⁵ H. E. Stanley, S. V. Buldyrev, M. Canpolat, O. Mishima, A. Sadr-Lahijany, M. R. Scala, and F. W. Starr, *Physical Chemistry and Chemical Physics* **2**, 1551 (2000).
- ⁵⁶ J. R. Errington, T. M. Truskett, and J. Mittal, *J. Chem. Phys.* **125**, 244502 (2006).
- ⁵⁷ J. E. Errington, P. G. Debenedetti, and S. Torquato, *J. Chem. Phys.* **118**, 2256 (2003).
- ⁵⁸ P. Camp, *Phys. Rev. E* **68**, 061506 (2003).
- ⁵⁹ M. R. Sadr-Lahijany, A. Scala, S. V. Buldyrev, and H. E. Stanley, *Phys. Rev. Lett.* **81**, 4895 (1998).